Summer 2022

Development of PEG-b-PLA Based Micelles for Neutralization of a Toxic Peptide

Giselle Campos
Missouri State University, Giselle97@live.missouristate.edu

As with any intellectual project, the content and views expressed in this thesis may be considered objectionable by some readers. However, this student-scholar's work has been judged to have academic value by the student's thesis committee members trained in the discipline. The content and views expressed in this thesis are those of the student-scholar and are not endorsed by Missouri State University, its Graduate College, or its employees.

Follow this and additional works at: https://bearworks.missouristate.edu/theses

Part of the Materials Chemistry Commons, Other Chemistry Commons, and the Polymer Chemistry Commons

Recommended Citation

DEVELOPMENT OF PEG-*b*-PLA BASED MICELLES FOR NEUTRALIZATION OF A

TOXIC PEPTIDE

A Master's Thesis

Presented to

The Graduate College of

Missouri State University

In Partial Fulfillment

Of the Requirements for the Degree

Master of Science, Chemistry

By

Giselle Campos

August 2022

DEVELOPMENT OF PEG-*b*-PLA BASED MICELLES FOR NEUTRALIZATION OF A TOXIC PEPTIDE

Chemistry

Missouri State University, August 2022

Master of Science

Giselle Campos

ABSTRACT

I herein report the preparation and characterization of PEG-*b*-PLA block copolymer micelles and PEG-*b*-PLA/PLA mixed micelles as potential "plastic antidotes" for a toxic peptide, melittin. PEG-*b*-PLA micelles have been used in a number of biomedical applications for their biodegradability and biocompatibility. Along these lines, I investigated the colloidal stability and the peptide absorption properties of PEG-*b*-PLA/PLA mixed micelles. A series of PEG-*b*-PLA block copolymer micelles and PEG-*b*-PLA/PLA mixed micelles were prepared, and their colloidal stability was studied. The hydrodynamic diameters of stable micelles were determined by using Dynamic Light Scattering (DLS). The capability of the micelles to capture and neutralize a hydrophobic toxic peptide derived from bee venom, melittin, was evaluated by hemolytic assay. The micelles consisting solely of PEG-*b*-PLA block copolymer were only found to inhibit melittin-induced hemolysis to a limited degree. Meanwhile, the micelles that consist of both PEG-*b*-PLA and PLA completely neutralize the effects of melittin. We attributed the contributing factor in melittin neutralization to the chemical nature of the micelle surface rather than the surface-to-volume ratio of the nanoparticle. The micelle mixture that exhibited the highest neutralization was comprised of 75% PLA and 25% PEG-*b*-PLA.

KEYWORDS: block copolymer micelles, FRET, melittin, PEG-PLA, synthetic antidote, toxin neutralization

DEVELOPMENT OF PEG-*b*-PLA BASED MICELLES FOR NEUTRALIZATION OF A

TOXIC PEPTIDE

By

Giselle Campos

A Master's Thesis
Submitted to the Graduate College
Of Missouri State University
In Partial Fulfillment of the Requirements
For the Degree of Master of Science, Chemistry

August 2022

Approved:

Keiichi Yoshimatsu, Ph.D., Thesis Committee Chair

Natasha DeVore, Ph.D., Committee Member

Gary Meints, Ph.D., Committee Member

Kyoungtae Kim, Ph.D., Committee Member

Julie Masterson, Ph.D., Dean of the Graduate College

ACKNOWLEDGEMENTS

TABLE OF CONTENTS

LIST OF TABLES

LIST OF FIGURES

INTRODUCTION

The use of nanoparticles in biological and biomedicine applications has been a growing area of interest in bioimaging,[1] drug delivery vehicles,[2] and toxin sequestration.[3] Of the three application areas that are mentioned above, the use of nanoparticles as antidotes for toxins has been a relatively less explored area. Therefore, there is a significant interest in developing a nanoparticle that can effectively capture and inhibit the target toxin without eliciting an immunological response.

As an example of nanoparticle-based antidotes, Zhang and coworkers reported the use of a biomimetic nanosponge to study its neutralization ability toward pore forming toxins (PFTs) such as α-toxin, streptolysin-O, and melittin.[4–6] These nanosponges are polylactic-co-glycolic acid (PLGA) nanoparticles wrapped with natural red blood cell bilayer membranes and serve as red blood cell decoys that are nonspecific in their toxin capture. Shea and coworkers reported a variety of N-isopropylacrylamide (NIPAm)-based hydrogel nanoparticles that are capable of neutralizing PFTs, snake venoms phospholipase A_2 (PLA_2) and three finger toxin (3FTX), peptide phenol-soluble modulin α3 (PSMα3), and melittin.[3,7–10] Koide and coworkers functionalized dipalmitoyl phosphatidylethanolamine (DPPE)-based lipid nanoparticles with select amino acids, polyethylene glycol (PEG), and a polymer ligand to optimize the neutralization efficiency against melittin and histones.[11–13]

As highlighted, these series of studies utilized an array of different materials as modes for toxin sequestration. However, it should be noted that little to no research has been conducted on the use of block copolymers for the capture of toxins. In this thesis, we are focused on the

potential utility of polyethylene glycol-block-polylactic acid (PEG-*b*-PLA) block copolymer

micelles and PEG-*b*-PLA mixed micelles as a potential plastic antidote for toxin neutralization.

PEG-*b*-PLA Block Copolymer Micelles

     Self-Assembly. Amphiphilic block copolymers such as PEG-*b*-PLA contain discrete

hydrophilic and hydrophobic blocks along the polymer chain, (Figure 1).
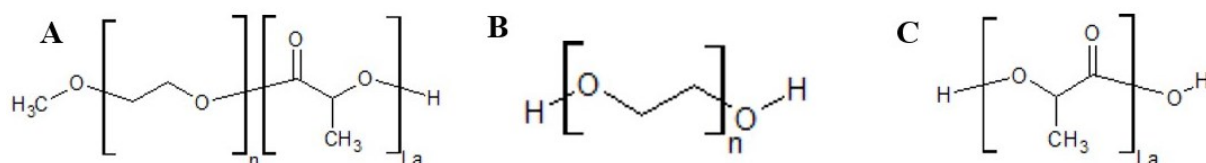
Figure 1. Chemical structures of A) polyethylene glycol-block-polylactic acid (PEG-*b*-PLA) B) polyethylene glycol (PEG) (hydrophilic) and C) polylactic acid (PLA) (hydrophobic).

     By having this characteristic, these polymers can self-assemble into different

nanostructures that vary in size and shape such as vesicles and cylindrical/spherical micelles in

aqueous solutions.[14–17] Figure 2 shows the different morphologies possible for amphiphilic

diblock copolymers. The block copolymer morphologies can depend a number of factors

including the structure of polymers, concentration, solvent, pH, and temperature.[15,16]
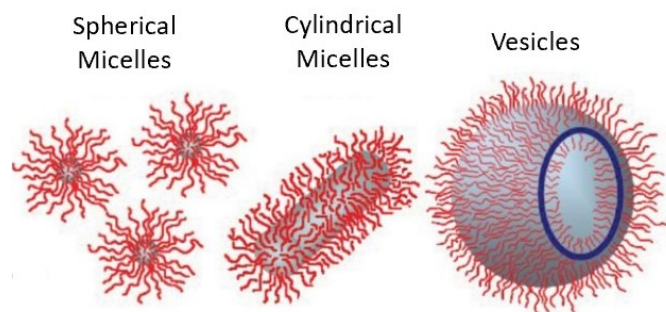
Figure 2. Different types of nanostructures for amphiphilic diblock copolymers. Adapted with permission from Reference [17].

Formation of spherical micelles is typically driven by the hydrophobic interactions between the hydrophobic blocks in the aqueous solution. The hydrophobic blocks assemble together to form a core whereas the hydrophilic blocks will form a surrounding hydrophilic shell.[18]

Applications. PEG-*b*-PLA block copolymers have been previously applied as a component of various biomaterials including implants[18] and surface coatings[19] for medical devices. Meanwhile, they have been most extensively investigated as vehicles for drug delivery due to their biocompatibility and biodegradability, and tunable size.[14,18,20,21] Since many therapeutics are hydrophobic in nature, upon spontaneous self-assembly of the polymer in aqueous solutions, the drugs can be incorporated into the hydrophobic core of the PEG-*b*-PLA micelle. By incorporating the drugs into the core, they can be transported at higher concentrations to circumvent water solubility issues and be released from the core in a controlled manner.[16,20] On the other hand, the hydrophilic shell serves to protect the hydrophobic core from protein adsorption and cellular adhesion, thus ultimately reducing fast elimination by host defenses and increasing blood circulation times.[16,18,20,21]

The effect of functionalization of shell structures has been another area of interest.[14] For example, Zhou *et al.*[22] prepared an array of different compositions of PLGA-PEG-maleimide (MAL) and combined it with PLGA-PEG in ratios and reacted the MAL with PEG-thiol to make two distinct PEG layers on the nanoparticle (Figure 3A). These two layers were called primary PEG and outer PEG layer and laid near the core and on the surface, respectively (Figure 3B). Where the primary PEG layer on nanoparticle surface exists in a brush conformation and the outer PEG layer forms a mushroom-to-brush conformation as PLGA-PEG-MAL percentage is increased. The primary PEG layer was reported to prevent the adsorption of proteins onto the

nanoparticle and the outer PEG layer could provide a topographically unique structure that would lead to long nanoparticle circulation.[22] By adding more percent PLGA-PEG-MAL, the nanoparticles made subsequently had an increased circulation time when compared to PLGA-PEG-only nanoparticles.
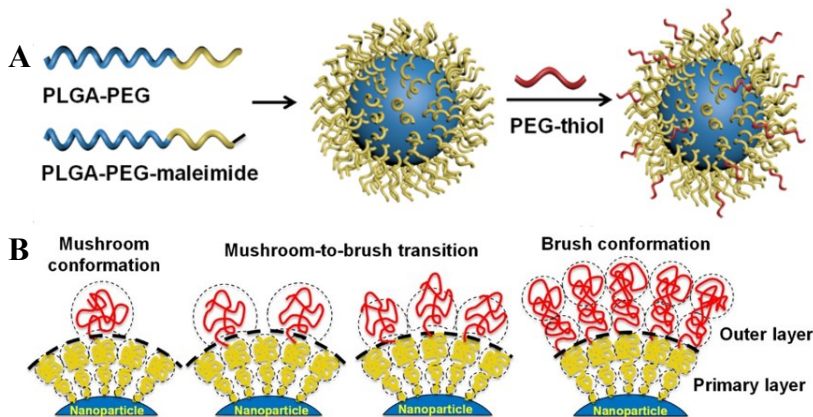
Figure 3. Representations of the unique topographical structure of the PEG shell. Adapted with permission from Reference [22].

Garofalo *et al.*[23] prepared multiple variations of "tree shaped" mPEG-(PLA)$_n$ block copolymers (n = 1, 2, or 4 arms of PLA; mPEG = 2 kDa or 5 kDa) through the use of a reaction scheme shown in Figure 4. These uniquely shaped branched mPEG-PLA copolymers were used to study how different copolymer structures would affect their stability in aqueous solutions and their efficiency in release of drug loads with tumor cells. These "tree shaped" polymers were utilized to prepare an array of micelles of different sizes and cell permeation abilities. While the authors reported the result of drug delivery for a limited number of micelles, one potential candidate for drug delivery was made, mPEG$_{2k}$-(PD,LLA)$_2$. The potential other candidates consisted of mPEG$_{5k}$-(PLLA), mPEG$_{5k}$-(PLLA)$_2$, and mPEG$_{2k}$-(PLLA) as these were able to associate but not enter the tumor cells in order to deliver paclitaxel.
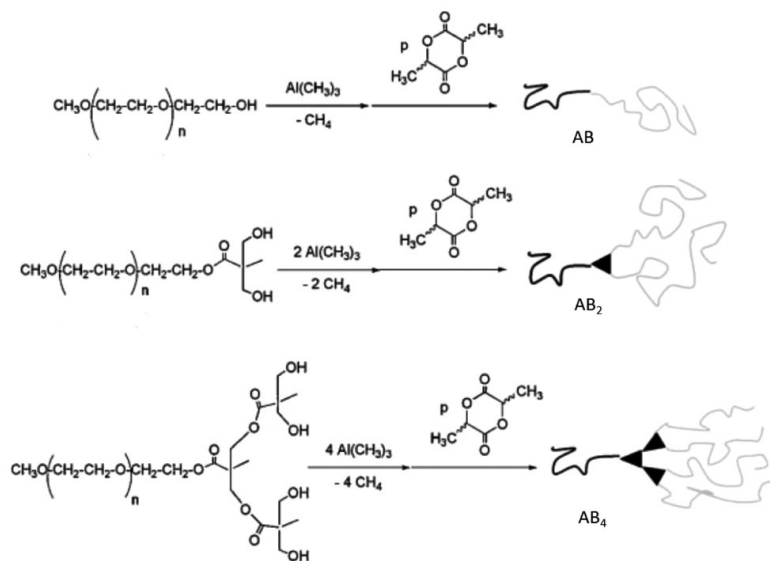
Figure 4. Synthesized "tree shaped" structure made from linear mPEG (A) and one to four PLA (B) arms. Reprinted with permission from Reference [23].

Förster Resonance Energy Transfer (FRET)

Fluorescence is the absorption of photons in the singlet ground state which are then stimulated to a singlet excited state and lead to the emission of a photon when it relaxes.[24] The spin of the excited electron is still paired with the ground state electron and as the excited molecule quickly returns to the ground state the emission of a photon is seen.[24] What should be noted is that the wavelength of the emitted photon is lower in energy (longer) than the initially absorbed photon due to a loss of energy. In general, fluorescence is dependent on the chemical structure of the molecule and typically occurs in conjugated molecules.[24]

Förster Resonance Energy Transfer (FRET) is a nonradiative electronic transfer of energy from an excited fluorophore (donor) to a ground state fluorophore (acceptor).[25,26] This process transfers the energy provided by the donor to excite the acceptor fluorophore. Thereafter, a radiative transfer (relaxation) in the form of a fluorescent emission occurs when the acceptor returns to the ground state. [25,26] The Jablonski diagram seen in Figure 5 provides a visual

explanation to the FRET process in terms of donor/acceptor excitation and emission.[27] In order for FRET to occur two criteria must be met, (1) there must be an integral overlap between the fluorescence emission spectrum of the donor and excitation spectrum of the acceptor fluorophore (2) the distance between the donor and acceptor fluorophores must fall in the range of $1 - 10$ nm.[25,26]
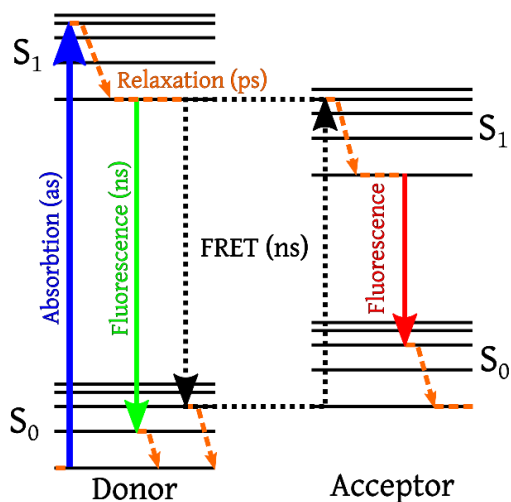
Figure 5. Demonstrating FRET and the energy transfer from the excited donor to the ground state acceptor via a nonradiative process (dashed black arrow). Reprinted with permission from Reference [27].

Due to its dependency to the donor-acceptor pair distance, FRET has been used in a wide variety of fields. In biology/medicine, FRET has been used to assess protein-protein interactions and conformation alteration of stimulated receptor and membranes.[25] Recently FRET has been utilized in material science/chemistry to monitor nanomedicine interactions with biological systems and provide information on *in vitro* and *in vivo* stability, intracellular drug release, as well as visualize biofate.[25] Along those lines the use of these fluorophores has been adapted to study the structural features of novel nanomaterials due to the reduced distance between the fluorophore upon assembly. FRET can also be used as a fluorescent probe to detect structural

dynamics of nanomaterials during the synthesis process (Figure 6A).[25] Construction of the

nanomaterial can be easily seen upon the increase of the acceptor peak and the reduction of the

donor peak. Or, vice versa, when the nanomaterial is introduced into the body via the

bloodstream, FRET can be used to monitor the overall structural integrity of the nanomaterial

(Figure 6B).[21,25,28] If the nanomaterial is compromised, the acceptor peak will abruptly reduce in

correlation to the increased of distance of the fluorophores. As for nanomaterials to be used in

medicine, the efficiency of drug/cargo loading and releasing is of great importance. With FRET,

loading and release can be monitored. If high FRET efficiency is seen the drugs/cargo were

properly loaded and if a low FRET efficiency is seen it leads to believe that the drug/cargo was

released (Figure 6C).[25,29,30]
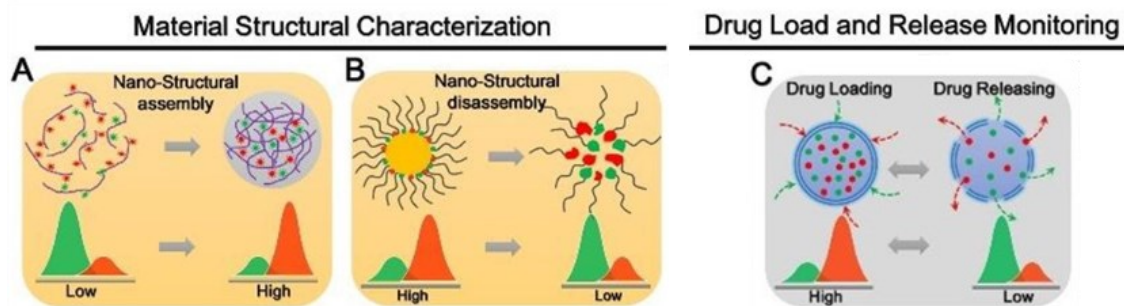
Figure 6. Examples of the use of FRET with nanomaterials. Adapted with permission from
Reference [25].

Toxins

An exposure to biological toxins can occur by either poisoning or envenoming. Poisons

cause harm through means of ingestion and injection and are typically made of small organic

molecules. Whereas venoms are only hazardous via injection and are composed commonly of

protein– and peptide based toxins.[31] Among these toxins, venoms are more elusive in terms of

their identity due to their diversity.[31,32] Some venoms are complex mixtures of a variety of toxins

and elicit physiological responses to compromise the enemy or prey, but the others may be made up of a relatively small number of components and only induce immediate pain.

Melittin. Melittin is a 26 amino acid cytolytic peptide; it constitutes 50% of the dry weight of venom from the European honey bee *Apis mellifera*.[33] Melittin is a common pore forming toxin (PFT) model used in research due to its consecutive positively charged and hydrophobic amino acids (Figure 7).[7–9,11,34] PFTs are the most commonly secreted bacterial and wild living creature toxins in nature.[4,5,35,36] These toxins are an essential factor in bacterial pathogenesis and open up a wide range of diseases and, as the name suggests, these toxins damage and compromise cell membranes by inducing pore formations via differing mechanisms.[5,7,32,35–38]

$^+$**GIGAVLK**$^+$**VL**TT**GLPALI**SWI**K**$^+$**R**$^+$**K**$^+$**R**$^+$QQ-CONH$_2$
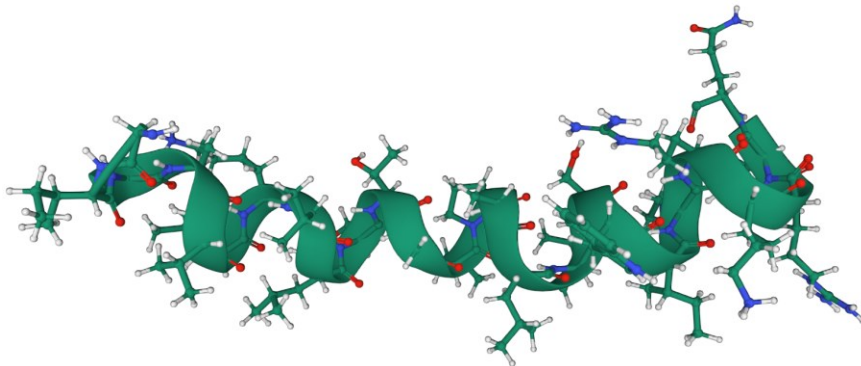
Figure 7. Structure and sequence of melittin. Blue indicates positively charged amino acid and brown indicates nonpolar amino acids.

As mentioned, melittin contains a majority of the hydrophobic residues near the amino-terminated region and the positively charged residues near the carboxyl-terminated region. This provides melittin with an amphiphilic property that makes it readily water-soluble.[9,11,33] Melittin

does not exert any biological activity by directly interacting with a specific receptor but rather works through a physical association with cell membranes, melittin can perpendicularly cork-screw into the cell creating perforations.[32,33,39] An effective strategy would be to inhibit melittin during circulation and cut their interaction with cell membranes by utilizing nanomaterials that capture the toxin on their surface or interior.[7,32]

Conventional Antivenom. The most common method of toxin neutralization is the administration of antiserums.[10,31,40] Antiserums are typically produced by the immunization of animals by intravenous injection of toxins or venoms as antigens. After the injection, the immune system of the animals respond to the antigens and produces the antibodies that bind to and neutralize the toxin or venom.[10,31] Although the antiserums produced by this method are known to work effectively, there is a risk of causing complications.[40] In some cases, antivenom-antiserum was reported to cause anaphylactic reactions through non-IgE or IgE, within 24 hours of administration.[31,40] Additionally, antivenom antibodies mixed with human anti-horse antibodies have also reported to extend half-life, which in turn could trigger inflammation and serum sickness in some cases.[31,32,40]

OBJECTIVE

Although many different nanomaterials have been investigated for the potential use in toxin sequestration, there has been little investigated on the use of PEG-*b*-PLA. In this study, I have focused on the preparation and characterization of PEG-*b*-PLA block copolymer micelles and PEG-*b*-PLA/PLA mixed micelles by dynamic light scattering, fluorescence spectroscopy, and a hemolytic neutralization assay. This block copolymer was chosen for its biodegradability and biocompatibility, two characteristics that are of great interest in biomedical applications.[14,18,20,21]

My hypothesis was that with the use of PEG-*b*-PLA and/or PEG-*b*-PLA/PLA mixed micelles, the adverse effects of a honeybee venom derived toxin, melittin, could be inhibited. By incorporating an optimized amount of PLA into the PEG-*b*-PLA block copolymer micelles, it would provide the nanoparticle with more hydrophobic and negative charges that would be complementary to melittin. The goal of this work was to investigate the stability and peptide absorption properties of PEG-*b*-PLA and/or PEG-*b*-PLA/PLA mixed micelles and study their potential utility as a "plastic antidote".

METHODS

Materials

Poly(D,L-lactide) acid endcap (5000-10,000) (M_n: 7,691 Da and M_w: 13,057 Da) (P(DL)LA) (PolySciTech Inc.), Poly(D,L-lactide) acid endcap (1000-5000) (M_n: 1,671 Da and M_w: 2,490 Da) (P(D)LA) (PolySciTech Inc.), Methoxy Poly(ethylene glycol)-*b*-Poly((D,L)lactide) Diblock (5,000:4,000, Da per block ratio), (M_n:11,862 Da and M_w:14,451 Da) (PolySciTech Inc.), Poly ((D,L)-lactide)-*b*-Poly(ethylene oxide)-*b*-Poly((D,L)-lactide) Triblock (5000:10,000:5000, Da per block ratio) (PolySciences Inc.) were used as received. Two fluorescent dyes, 1,1′-Di-*n*-octadecyl-3,3,3′,3′-tetramethylindocarbocyanine perchlorate (DiI) and 3,3′-dioctadecyloxacarbocyanine perchlorate (DiO), were purchased from Alfa Aesar by Thermo Fisher Scientific and Biotium, respectively. Acetone (Reagent Grade) and Water (HPLC Grade, Fisher Scientific) was used to prepare micelle stock solutions. Melittin from honeybee venom, ≥85% (Sigma) and Bovine Red Blood Cells, 10% (Lampire Biological Laboratories) were used in hemolytic neutralization assays.

Experimental

UV-Vis Measurements. <u>Dye Concentration Quantification.</u> Stock concentrations of DiO (donor) and DiI (acceptor) were prepared by dissolving approximately 1 mg of DiO or DiI in 1 mL of acetone in a 1.5 mL centrifuge tube and stored at 4 °C. The concentration of each dye was determined via absorption on a Cary 60 Spectrophotometer (Agilent Technologies). Each dye was diluted to 1/1000 in acetone and placed in a 1.5 mL glass cuvette and the absorption was measured in 1 nm intervals over a 400 – 650 nm range. Molar coefficients used to quantify the

concentration were $\varepsilon_{484} = 154,000\ M^{-1}cm^{-1}$ and $\varepsilon_{549} = 148,000\ M^{-1}cm^{-1}$, respectively for DiO and DiI.

Preparation of Block Copolymer Micelles. All micelles were prepared by dissolving approximately 10 mg of the desired polymer(s) in 0.5 mL of acetone and placed in a 1.5 mL centrifuge tube. To aid in dissolving, shaking and venting of the centrifuge tube was performed. FRET micelles (micelles with both dyes incorporated into the core) were prepared by adding approximately 0.075 mg of DiI (0.75% wt/polymer wt) and 0.015 mg of DiO (0.15% wt/polymer wt) to the 0.5 mL solution. The resulted solution was added to a 20 mL borosilicate scintillation vial containing 5 mL of HPLC grade water, dropwise, and mixed at 300 rpm for 3 hours to evaporate the acetone and facilitate the formation of micelles and the uptake of the dyes. After preparation, the solution was removed from mixing and all samples prepared were wrapped in aluminum foil and stored at room temperature.

Fluorescence Measurements including FRET measurement. All fluorescence measurements were measured on a QuantaMaster spectrofluorometer (Photon Technology International, Inc.) at a concentration of 0.005 mg mL^{-1} in 3 mL aliquots in a quartz cuvette. For the measurements of the emission spectra of DiO and FRET, the cuvette containing a liquid sample was exposed to an excitation wavelength of 425 nm and emission over 450 - 650 nm was measured. For measurements of the emission spectra of DiI, the sample was exposed to an excitation wavelength of 475 nm and emission over 500 – 700 nm was measured. The excitation spectra for DiO/FRET and DiI were measured using emission wavelength of 570 nm and 625 nm, respectively. All fluorescent measurements were measured in 1 nm intervals and the slit widths for the excitation and emission windows were set to 8 nm and 10 nm, respectively.

Hemolytic Activity Neutralization Assay. Red blood cells (RBCs) were washed with phosphate-buffered saline (PBS; 35 mM phosphate buffer/0.15 M NaCl, pH 7.3), collected by centrifugation (10 min, 800 g), and then resuspended in PBS three times. 1.8 µM melittin (final concentration in RBC solution) was preincubated with the micelles for 15 min at 37 °C in PBS. The RBC solution (100 µL) was added to the melittin/micelle mixture to give a final volume of 200 µL. The final solution was incubated at 37 °C for 15 min and was then centrifuged at 3000 g for 10 min. Release of hemoglobin was monitored by measuring the absorbance (A_{sample}) of the supernatant at 415 nm on a NanoDrop One^c (Thermo Scientific). Controls for 0% and 100% neutralization of hemolytic activity consisted of RBCs incubated with 1.8 µM melittin without micelles ($A_{0\%}$) and RBC suspension without melittin and micelles ($A_{100\%}$), respectively. Figure 8 provides a simplified outline of the procedures for the assay. The percentage of neutralization was calculated according to Equation 1 below.
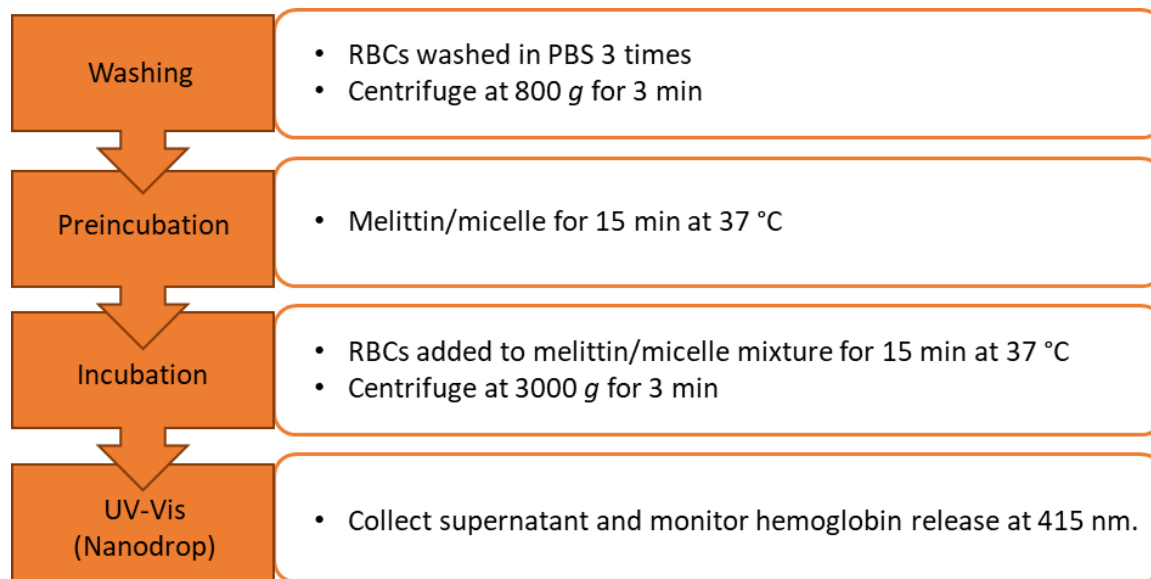
Figure 8. Outline of the procedure for the hemolytic neutralization assay.

$$\text{Neutralization \%} = \frac{A_{sample} - A_{0\%}}{A_{100\%} - A_{0\%}} \times 100 \tag{1}$$

Dynamic Light Scattering (DLS). All dynamic light scattering measurements were measured on a NanoBrook Omni (Brookhaven Instruments) at a concentration of 0.02 mg mL^{-1} for each stock in 3 mL aliquots in a plastic cuvette. The cuvette was maintained at 25 °C and exposed to a wavelength of 640 nm and a scattering angle of 90 °. All analyses were repeated three times per each sample. Using the hydrodynamic diameter (d_h), the surface area-to-volume ratio was calculated using Equation 2 below.

$$\text{surface area} - \text{to} - \text{volume ratio} = \frac{4\pi\left(\frac{d_h}{2}\right)^2}{\frac{4}{3}\pi\left(\frac{d_h}{2}\right)^3} \tag{2}$$

RESULTS AND DISCUSSION

Colloidal Stability of PEG-*b*-PLA Block Copolymer Micelles

Melittin contains residues that are hydrophobic and positively charged. To make micelles that interact with the melittin in solution, PLA was added during the preparation. This PLA homopolymer provides additional hydrophobicity to the micelle as well as some negative charge from the free carboxyl group on the end of the segment. PEG-*b*-PLA block copolymer (consisting of with 5.0 kg PEG block/mol and 4.0 kg PLA block/mol) and PLA homopolymer (7.7 kg/mol) were solubilized in acetone together in compositions of 10 mg maxima per 0.5 mL of acetone. The compositions were based on polymer weight ratios between the block copolymer and homopolymer. The studied compositions were 100%:0%, 75%:25%, 50%:50%, 25%:75% and 0%:100% (block copolymer: homopolymer). These compositions were chosen in order to gauge the micelles' colloidal stability, as the addition of the PLA homopolymer could disrupt the micelle formation. This was to identify an optimized ratio between the amount of PEG and PLA to prepare colloidally stable micelles with melittin binding capability. When less PEG and more PLA are incorporated, the micelles would less likely exhibit a stable hydrophilic shell for to retaining the micelle shape but more likely would adsorb peptides. Additionally, the inverse is equally a concern, incorporation of more PEG and less PLA could likely improve the stability of micelles but at a cost of reduced peptide binding capability. These specific block copolymer/homopolymer compositions were investigated as they provide an easy benchmark where modifications can be accomplished.

Figure 9 shows the fluorescent spectra of DiO and DiI dyes in acetone. This donor-acceptor fluorophore pair (DiO and DiI) was used to confirm the formation of micelles, which

allows for the colocalization of the dyes in the hydrophobic core. In this work, the donor and

acceptor peaks at 505 nm and 565 nm, respectively, was used to study the occurrence of FRET

as previously reported in literature.[41] The spectra also showed an overlap in the emission

spectrum of DiO (measured with excitation light of 425 nm) and excitation spectrum of DiI

(measured at emission light of 625 nm), which is required for FRET. Additionally, it shows that

the excitation at 425 nm minimizes the direct excitation of DiI by the excitation light.
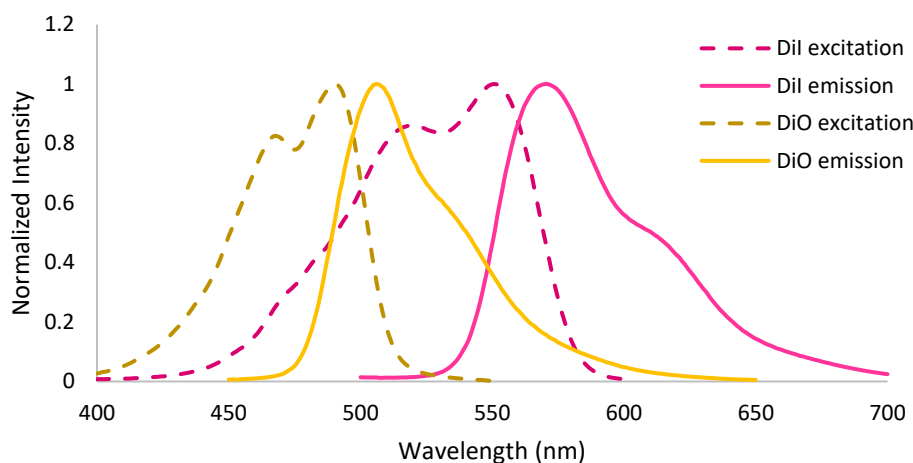
Figure 9. Normalized fluorescent spectra of micelles containing DiO (donor, yellow) and DiI (acceptor, pink) dyes.

The portion of this study focused on the use of PLA 7.7 kg/mol to prepare colloidally

stable micelles, all combinations for micelles containing PLA 7.7 kg/mol are seen in Table 1 and

are denoted as FM to indicate FRET micelles, micelles containing the fluorescent dyes. To

monitor micellular-like formation, the presence of the FRET peak was observed. The formation

of a FRET peak on the spectrum indicates incorporation of the hydrophobic dyes into the

micelle's core within a 10 nm distance from one another.

Table 1. Library of PEG-*b*-PLA diblock copolymer/PLA 7.7 kg/mol micelles utilized for fluorescence measurement.

Micelle ID Code	Polymer Composition (weight %)		Observed Precipitates (Y/N)
	PEG-*b*-PLA Diblock	PLA (7.7 kg/mol)	
FM 21	75	25	N
FM 22	50	50	N
FM 23	25	75	N
FM 14	0	100	Y

Studies were performed on PLA 7.7 kg/mol 100% (FM 14), Diblock 75%:PLA 7.7 kg/mol 25% (FM 21), Diblock 50%:PLA 7.7 kg/mol 50% (FM 22), and Diblock 25%:PLA 7.7 kg/mol 75% (FM 23) in order to observe the initial behavior of the dyes with these compositions. Initially, PLA 7.7 kg/mol 100% exhibited a fluorescent peak analogous to a FRET peak. A plausible explanation for this could be due to the presence of PLA precipitates, since PLA is hydrophobic in water, when the solution was being prepared rather than becoming micelles an opaque PLA suspension was made. Within that suspension the hydrophobic dyes adhered to the suspended PLA within a close enough proximity to each other and caused a pseudo-FRET peak to appear. In all cases of the Diblock and PLA homopolymer combinations a FRET peak was present (Figure 10). No adverse effects pertaining to the micelle's ability to form were seen due to adding the PLA 7.7 kg/mol chain to the Diblock copolymer, indicating that this method is able to produce stable micelles.
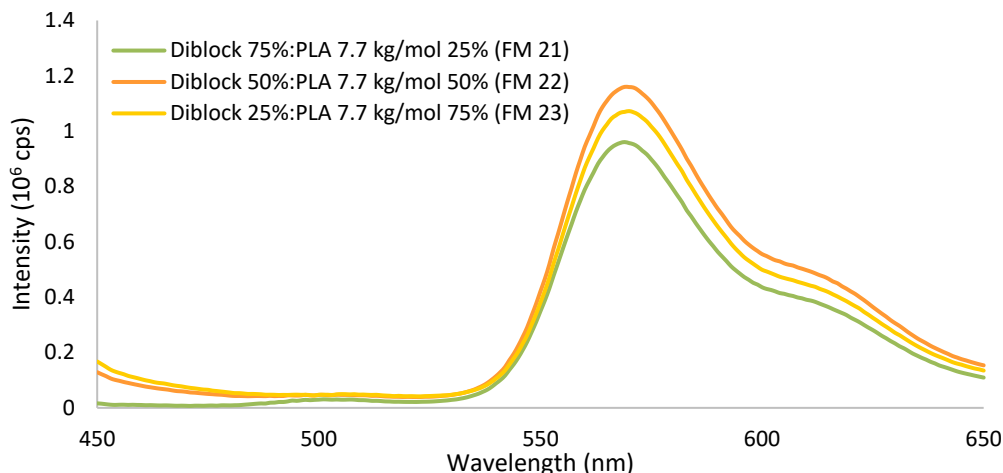
Figure 10. Fluorescence spectra of micelles consisting of Diblock copolymer and long chain PLA (FM 21, FM 22, and FM 23).

Micelle Characterization

The diameter of the Diblock:PLA mixed micelles measured by DLS are summarized in Table 2. It was seen that Diblock 100%:PLA 7.7 kg/mol 0% had the smallest diameter of all the samples as, due to its small size, was not able to be detected by the DLS. But as the PLA weight increased per sample, so did the diameter of the micelles. Such that Diblock 25%:PLA 7.7 kg/mol 75% had the largest recorded diameter of 114.49 nm.

Table 2. Size Distribution of Diblock:PLA mixed micelles.

Micelle	Hydrodynamic Diameter (nm)
Diblock 100%:PLA 7.7 kg/mol 0%	n.d.[a]
Diblock 75%:PLA 7.7 kg/mol 25%	72.22 ± 2.72
Diblock 50%:PLA 7.7 kg/mol 50%	97.01 ± 0.35
Diblock 25%:PLA 7.7 kg/mol 75%	114.49 ± 0.39

[a]Not determinable by DLS.

The surface-to-volume ratio of each micelle was also calculated and reported in Table 3. It should be noted that the surface area-to-volume ratio of the micelle decreases as the diameter of micelle increases. This means that the micelles with larger diameters have less surface area available for binding of peptides.

Table 3. Surface area to volume ratio of each micelle mixture.

Micelle	Surface Area to Volume Ratio (nm^2/nm^3)
Diblock 100%:PLA 7.7 kg/mol 0%	n.d.
Diblock 75%:PLA 7.7 kg/mol 25%	0.08311
Diblock 50%:PLA 7.7 kg/mol 50%	0.06184
Diblock 25%:PLA 7.7 kg/mol 75%	0.05240

Neutralization Assay

To test the micelle's ability to neutralize the hemolytic effects of melittin, empty micelle (EM) analogs were prepared using the same polymer compositions. All combinations used for the hemolytic neutralization assays are seen in Table 4.

Table 4. Library of micelles utilized for neutralization assays.

Micelle ID Code	Polymer Composition (weight %)	
	Diblock	PLA (7.7 kg/mol)
EM 28	100	0
EM 24	75	25
EM 25	50	50
EM 26	25	75

An initial comparison of the naked block copolymers was conducted to gauge their neutralization efficiency without any PLA 7.7 kg/mol polymer. Figure 11 shows the results of the hemolytic assay that include the photo of the supernatant. The micelles consisting of solely Diblock copolymer can only neutralize up to 60% of the hemolytic effect of melittin in solution at the concentration of 1.2 mg polymer mL^{-1}. In contrast, the PEG-*b*-PLA/PLA 7.7 kg/mol mixed micelles could completely inhibit melittin. By incorporating PLA, there was an increase in neutralization by 30% or more with the addition of only 25% PLA (Figure 11). It was seen that Diblock 25%:PLA 7.7 kg/mol 75% (EM 26) exhibited the highest percent neutralization at 99%. EM 26 micelle happens to be the micelle that is largest in diameter, providing evidence that melittin neutralization efficiency is not primarily determined by particle size and surface area but the properties of the micelle surfaces.
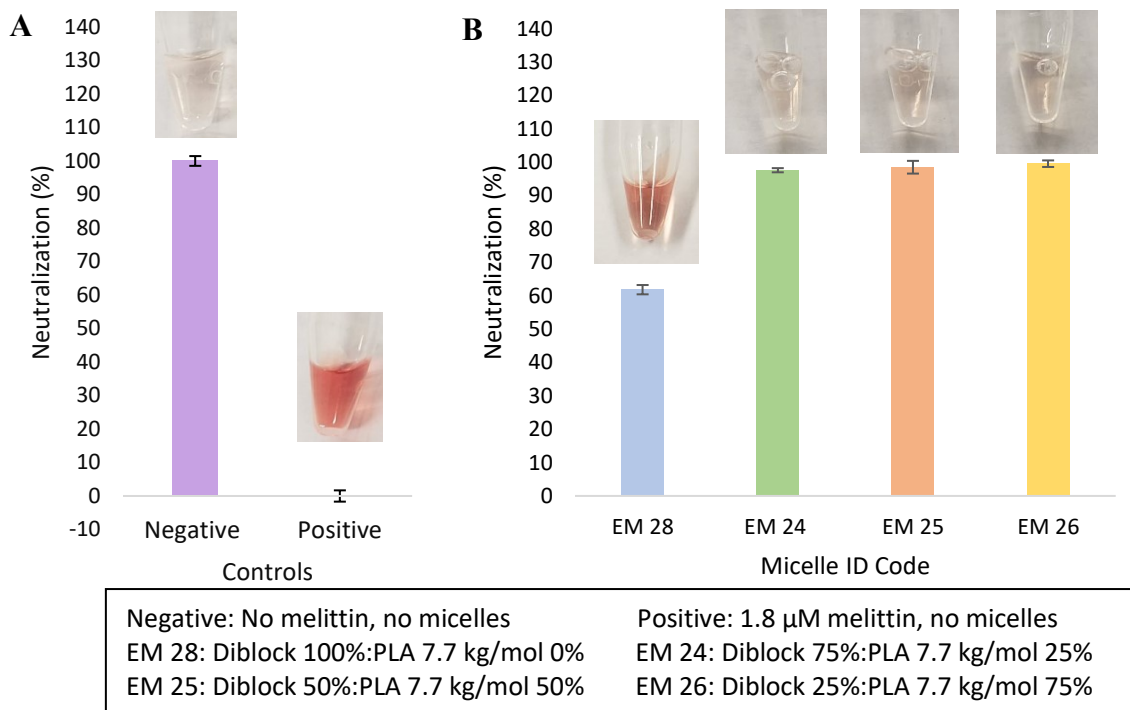
Figure 11. Neutralization quantification of melittin (1.8 µM) by EM 28, EM 24, EM 25, and EM 26 micelles (1.2 mg polymer mL^{-1}).

In order to confirm that the micelles do not show any adverse effect toward RBCs, the amount of hemolysis was measured in incubation of micelles with RBC alone. The same assay procedure that was used in for the neutralization assay was performed without the presence of melittin, and the results are shown in Table 5. It was seen that with none of the three micelle mixtures showed any hemolytic activity.

Table 5. Lack of polymer induced hemolysis in absence of melittin.

Micelles	Average Percent Neutralization	Standard Deviation
EM 24	101.3	0.0966
EM 25	100.6	0.329
EM 26	101.0	0.959

To further study neutralization capabilities of the micelles, the melittin neutralization efficacy was measured at three different micelle concentrations: 0.012, 0.12, and 1.2 mg mL^{-1}. While the concentration of melittin was kept constant at 1.8 µM. The neutralization trend based on micelle concentration is shown in Figure 12. All samples containing 0.012 mg mL^{-1} had a neutralization less than or equal to 10% and samples containing 0.12 mg mL^{-1} or above of micelles exhibited neutralization greater or equal to 80%. Regardless of micelle concentration, it was seen that with a larger percent of PLA 7.7 kg/mol present in the micelle the larger the neutralization, this is seen around 0.12 mg mL^{-1}. It was also observed that the % neutralization of melittin exhibited a sharp increase from 10 to 80% neutralization when the micelle concentration was increased from 0.012 to 0.12 mg mL^{-1}. Therefore, I next investigated the melittin neutralization efficacy of these micelles at six different concentrations ranging from 0.0102 to 0.204 mg mL^{-1}.
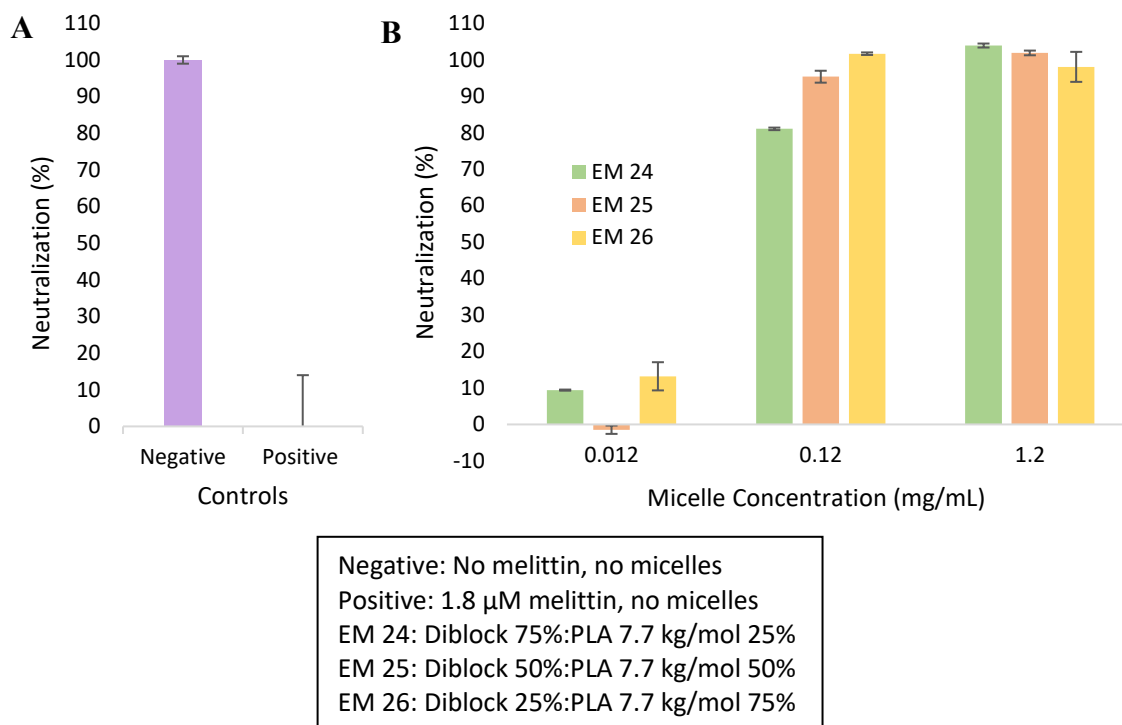
Figure 12. Neutralization quantification of melittin (1.8 µM) by differing concentrations of EM 24, EM 25, and EM 26 micelles.

As seen in Figure 13, all samples containing 0.204 mg mL^{-1} provided the maximum melittin-neutralization capability for each micelle mixture. Diblock 50%:PLA 7.7 k 50% and Diblock 25%:PLA 7.7 k 75% both exhibited approximately 100% neutralization. Whereas Diblock 75%:PLA 7.7 kg/mol 25% and Diblock 100%:PLA 7.7 kg/mol 0% exhibited only ~90% and ~50% neutralization, respectively, at the concentration of 0.204 mg mL^{-1}. At lower concentrations, melittin neutralization efficacy of all four micelles gradually decreased in a concentration-dependent manner. Diblock 50%:PLA 7.7 kg/mol 50% and Diblock 25%:PLA 7.7 kg/mol 75% micelles consistently neutralized more than 90% melittin-induced hemolysis at 0.072 mg mL^{-1} or higher micelle concentrations, whereas Diblock 75%:PLA 7.7 kg/mol 25% and Diblock 100%:PLA 7.7 kg/mol 0% micelles showed significant less melittin neutralization capability at the same concentration.

Table 6 summarizes the concentration of each micelle mixture that are required to neutralize 50% of melittin-induced hemolysis. As it can be seen, Diblock 50%:PLA 7.7 kg/mol 50% (EM 25) and Diblock 25%:PLA 7.7 kg/mol 75% (EM 26) exhibited the most effectively neutralized melittin. It is noteworthy that EM 25 and EM 26 are the two largest micelles in diameter and provide a smaller surface area-to-volume ratio for melittin binding. Therefore, our results indicated that the melittin neutralization efficacy is dependent on the properties of the surface of the micelles and rather than the simple differences on their surface areas.
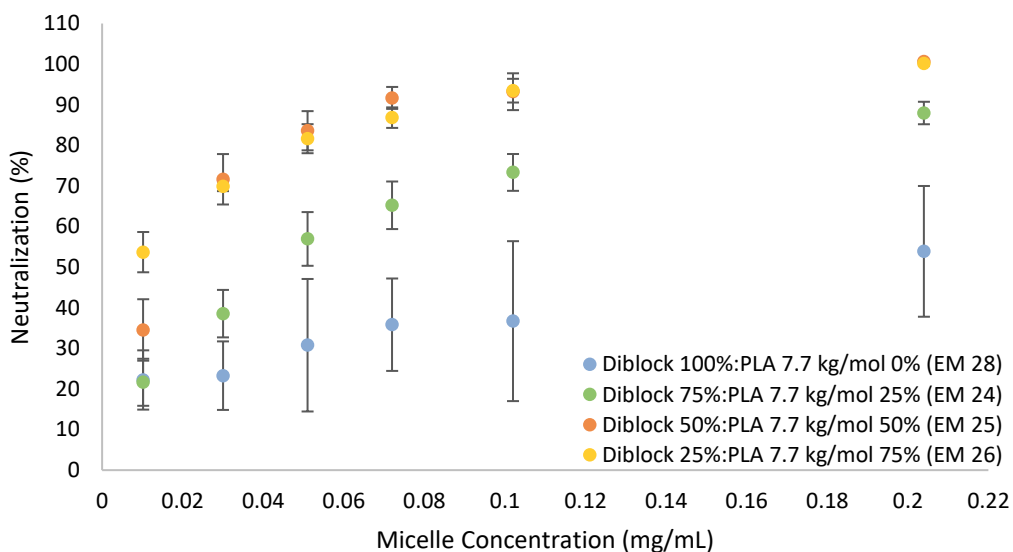
Figure 13. Neutralization with differing micelle concentrations (0.0102 – 0.204 mg mL^{-1}).

Table 6. Concentration of micelles needed to achieve 50% toxin inhibition.

Micelle	50% Neutralization Concentration (mg mL^{-1})
Diblock 100%:PLA 7.7 kg/mol 0%	0.180
Diblock 75%:PLA 7.7 kg/mol 25%	0.042
Diblock 50%:PLA 7.7 kg/mol 50%	0.018
Diblock 25%:PLA 7.7 kg/mol 75%	<0.0102

As it was shown, among the four combinations, Diblock 50%:PLA 7.7 kg/mol 50% and Diblock 25%:PLA 7.7 kg/mol 75% exhibited the highest melittin neutralization even at the low polymer concentration range. To further study the melittin neutralization efficacy at the low polymer concentration range, hemolysis assay was then performed with lower polymer concentrations (between 0.003 and 0.03 mg mL^{-1}). As shown in Figure 14 at 0.03 mg mL^{-1} the neutralization efficacy of Diblock 50%:PLA 7.7 kg/mol 50% and Diblock 25%:PLA 7.7 kg/mol 75% micelles begin to deviate from each other. At the low polymer concentration range, Diblock 25%:PLA 7.7 kg/mol 75% micelles exhibited slightly higher capability to neutralize melittin.
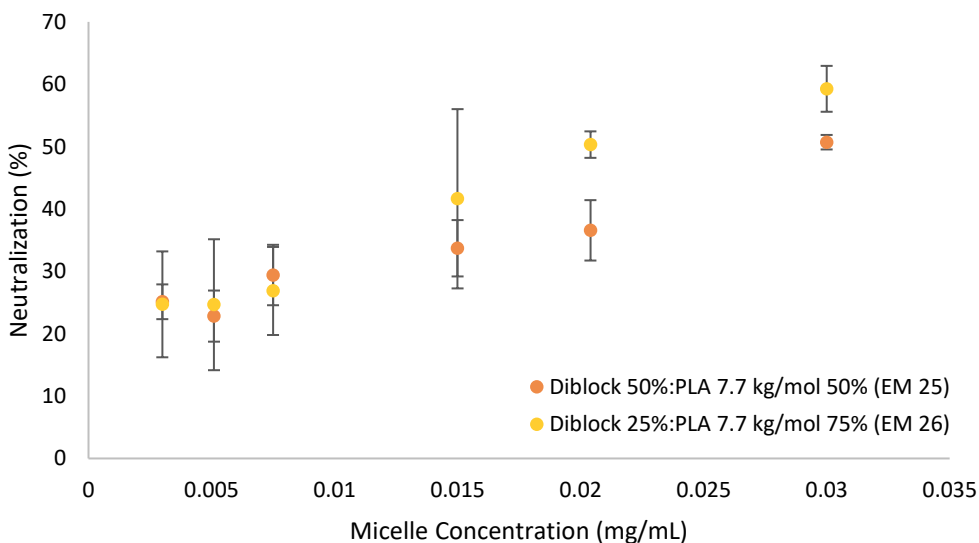
Figure 14. Neutralization with micelles at lower concentrations (0.0030 – 0.030 mg mL^{-1}).

Effectiveness of PLA-PEG-PLA Triblock Copolymer-Based Micelles in Melittin Neutralization

In addition to PEG-*b*-PLA diblock copolymer-based micelles, a Triblock copolymer, PLA-*b*-PEG-*b*-PLA (5 kg/block:10 kg/block:5 kg/block) micelles were prepared and evaluated by hemolytic assay. Herein, PLA with a shorter molar mass (1.7 kg/mol) was also incorporated into the micelles. As shown in Table 7, all combinations for micelles containing PLA 1.7 kg/mol

and PLA 7.7 kg/mol. Similar to behaviors seen previously by PLA 7.7 kg/mol, PLA 1.7 kg/mol

alone created an opaque hydrophobic suspension in the aqueous solution. When the PLA was

mixed with the Triblock, no precipitants were seen. As shown in Figure 15, a FRET peak was

seen in all cases of the Triblock:PLA 1.7 kg/mol homopolymer combinations. No adverse effects

pertaining to the micelle's ability to form was observed, similar to what was seen with the

Diblock.

Table 7. Library of PLA-*b*-PEG-*b*-PLA triblock copolymer/PLA micelles utilized for fluorescence measurement.

Micelle ID Code	Polymer Composition (weight %)			Observed Precipitates (Y/N)
	Triblock	PLA (1.7 kg/mol)	PLA (7.7 kg/mol)	
FM 13	100	0	0	N
FM 12	75	25	0	N
FM 10	50	50	0	N
FM 8	0	100	0	Y
FM 16	75	0	25	N
FM 15	50	0	50	N
FM 17	25	0	75	N
FM 14	0	0	100	Y

Although all the PLA 1.7 kg/mol chain length mixtures could be used to prepare stable

mixed micelles, it was noted that the melting temperature of the PLA 1.7 kg/mol homopolymer

appeared to be lower than room temperature. This was noticed due to the fact that PLA 1.7

kg/mol homopolymer melted during weighing. Based on this observation, our conclusion was that PLA homopolymer with a longer chain length (PLA 7.7 kg/mol) should form micelles that are more stable at physiological temperatures. As it is shown in Figure 16, all micelle mixtures showcased the FRET peak, indicating that stable micelles were prepared.
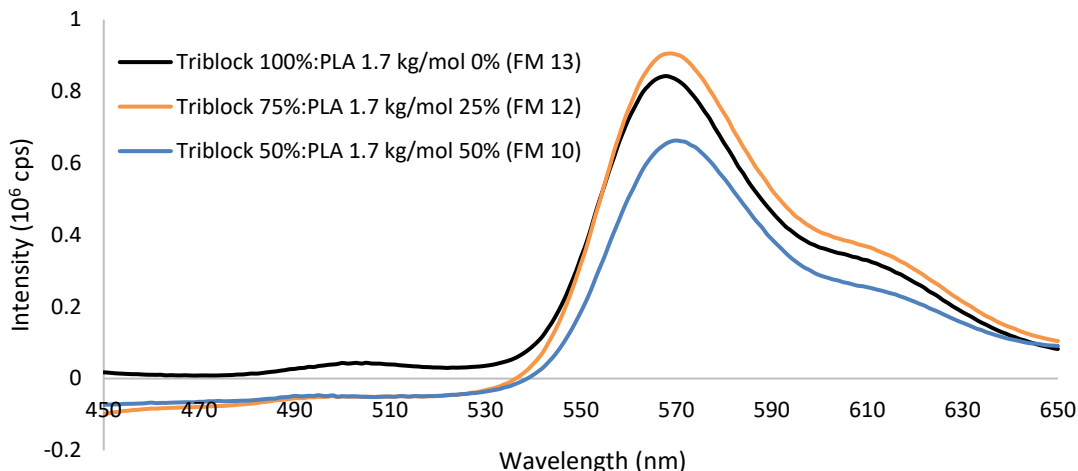
Figure 15. Fluorescence spectra of micelles consisting of Triblock copolymer and short chain PLA (FM 13, FM 12, and FM 10).
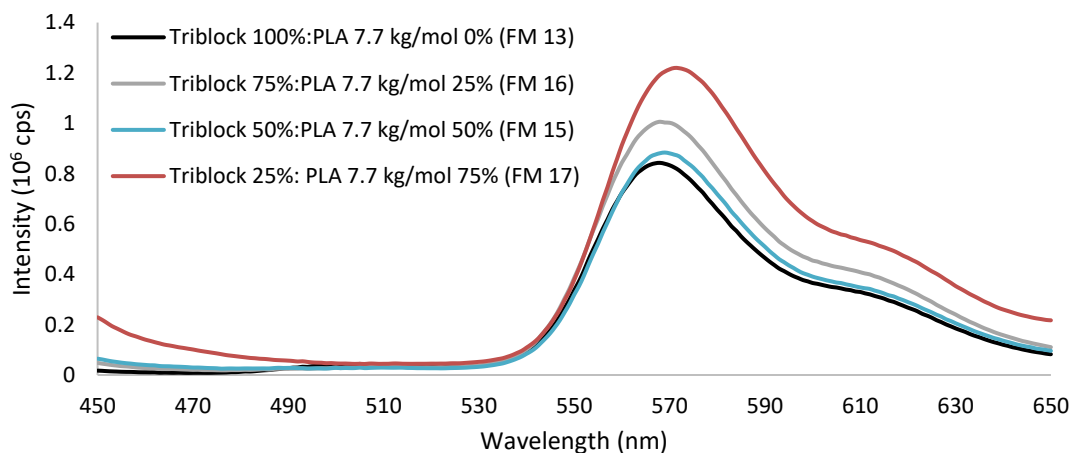
Figure 16. Fluorescence spectra of micelles consisting of Triblock copolymer and long chain PLA (FM 13, FM 16, FM 15, and FM 16).

To gauge the melittin neuralization efficiency, the Triblock copolymer micelle was compared with Diblock copolymer micelles. As it can be seen on the results in Figure 17, PLA-*b*-PEG-*b*-PLA Triblock copolymer micelles were able to fully neutralize the hemolytic toxicity of melittin when Diblock micelles at 1.2 mg polymer mL^{-1} only neutralized up to 60%. This result demonstrated the potentially superior property of PLA-*b*-PEG-*b*-PLA Triblock copolymer micelles as a platform for the development of a new melittin-neutralization antidote.

Negative: No melittin, no micelles   Positive: 1.8 µM melittin, no micelles
EM 27 Triblock 100%:PLA 7.7 kg/mol 0%   EM 28: Diblock 100%:PLA 7.7 kg/mol 0%
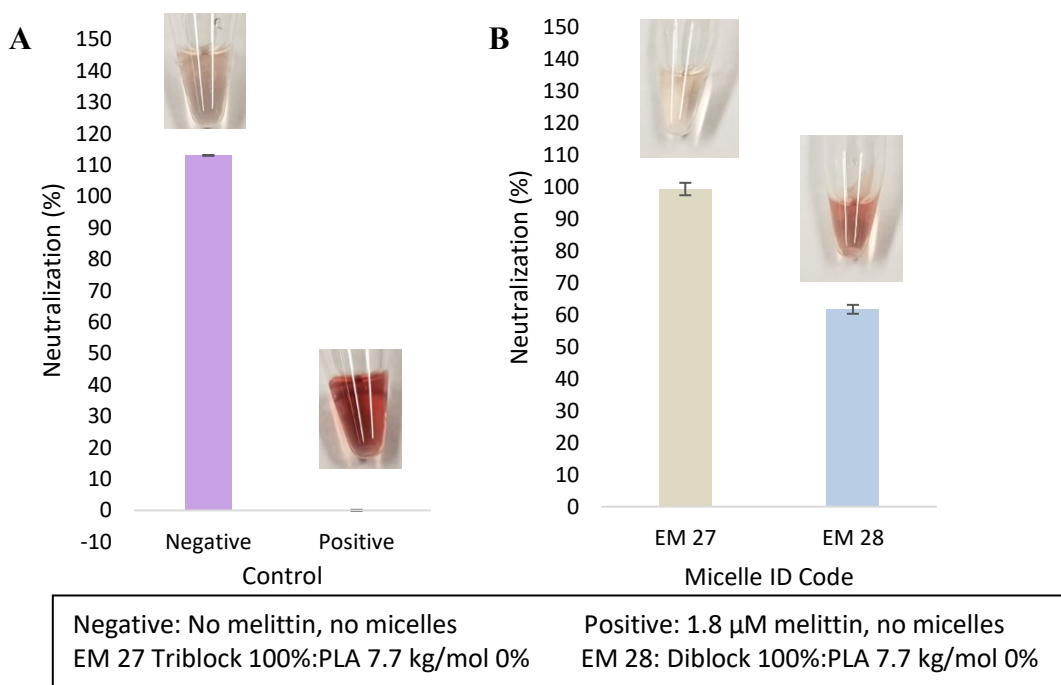
Figure 17. Neutralization quantification of melittin (1.8 µM) by EM 27 and EM 28 micelles (1.2 mg polymer mL^{-1}).

Overall, this work showcased that PEG-*b*-PLA/PLA mixed micelles can be prepared and used as a potential "plastic antidotes" for melittin. Diblock:PLA mixed micelles was shown to effectively neutralized melittin. Additionally, a micelle consisting of triblock copolymer alone showed a high potential as plastic antidote for melittin-neutralization.

CONCLUSION

This work demonstrated the potential utility of PEG-*b*-PLA block copolymer micelles and PEG-*b*-PLA block copolymer/PLA mixed micelles for capturing and neutralizing melittin. The micelles have their PEG segment on the surface and hydrophobic PLA segment in their interior. The PEG segment provides colloidal stability for the micelle and the PLA exhibits hydrophobic and, to a limited extent, negative charges. Our design was to optimize melittin-binding affinity through the optimization of the PEG to PLA ratio. The initial part of the work focused on studying how the PEG to PLA ratio would affect the colloidal stability and the size of micelles. All combinations, Diblock 75%:PLA 7.7 kg/mol 25%, Diblock 50%:PLA 7.7 kg/mol 50%, and Diblock 25%:PLA 7.7 kg/mol 75% formed stable micelles. It was established through neutralization assays that the neutralization efficacy of the micelles was greatly increased with just a 2.5 mg addition of PLA homopolymer. With Diblock 50%:PLA 7.7 kg/mol 50% and Diblock 25%:PLA 7.7 kg/mol 75% effectively neutralizing 50% of the melittin in solution with concentrations of 0.018 and <0.0102 mg mL^{-1}, respectively. The micelle mixture that exhibited the highest melittin neutralization capability, Diblock 25%:PLA 7.7 kg/mol 75%, had the largest diameter, indicating that the melittin capture is not due to the variations in available surface areas. This supports our hypothesis that the optimization of PEG-*b*-PLA to PLA ratio would provide optimal characteristics of micelles for efficient neutralization of melittin. Additional studies were conducted with a Triblock copolymer and varying sizes of PLA homopolymer. Colloidally stable micelles were made with either PLA length but considering the physiological temperature, we opt to use a 7.7 kg/mol PLA rather than 1.7 kg/mol PLA as it was more stable. When it came to neutralization studies, the Triblock captured and neutralized all the melittin and

28

did not need modifications with PLA. This work established the potential of colloidally stable polymer-based micelles as "plastic antidotes" for neutralization of toxic peptides, suggesting a new avenue for developing promising alternatives to conventional antidotes.

REFERENCES

(1)   Han, X.; Xu, K.; Taratula, O.; Farsad, K. Applications of Nanoparticles in Biomedical Imaging. *Nanoscale* **2019**, *11* (3), 799–819. https://doi.org/10.1039/c8nr07769j.

(2)   Patra, J. K.; Das, G.; Fraceto, L. F.; Campos, E. V. R.; Rodriguez-Torres, M. del P.; Acosta-Torres, L. S.; Diaz-Torres, L. A.; Grillo, R.; Swamy, M. K.; Sharma, S.; Habtemariam, S.; Shin, H.-S. Nano Based Drug Delivery Systems: Recent Developments and Future Prospects. *J. Nanobiotechnology* **2018**, *16* (1), 71. https://doi.org/10.1186/s12951-018-0392-8.

(3)   O'Brien, J.; Shea, K. J. Tuning the Protein Corona of Hydrogel Nanoparticles: The Synthesis of Abiotic Protein and Peptide Affinity Reagents. *Acc. Chem. Res.* **2016**, *49* (6), 1200–1210. https://doi.org/10.1021/acs.accounts.6b00125.

(4)   Hu, C.-M. J.; Fang, R. H.; Copp, J.; Luk, B. T.; Zhang, L. A Biomimetic Nanosponge That Absorbs Pore-Forming Toxins. *Nat. Nanotechnol.* **2013**, *8* (5), 336–340. https://doi.org/10.1038/nnano.2013.54.

(5)   Chen, Y.; Chen, M.; Zhang, Y.; Lee, J. H.; Escajadillo, T.; Gong, H.; Fang, R. H.; Gao, W.; Nizet, V.; Zhang, L. Broad-Spectrum Neutralization of Pore-Forming Toxins with Human Erythrocyte Membrane-Coated Nanosponges. *Adv. Healthc. Mater.* **2018**, *7* (13), 1701366. https://doi.org/10.1002/adhm.201701366.

(6)   Chen, Y.; Zhang, Y.; Chen, M.; Zhuang, J.; Fang, R. H.; Gao, W.; Zhang, L. Biomimetic Nanosponges Suppress In Vivo Lethality Induced by the Whole Secreted Proteins of Pathogenic Bacteria. *Small* **2019**, *15* (6), 1804994. https://doi.org/10.1002/smll.201804994.

(7)   Hoshino, Y.; Urakami, T.; Kodama, T.; Koide, H.; Oku, N.; Okahata, Y.; Shea, K. J. Design of Synthetic Polymer Nanoparticles That Capture and Neutralize a Toxic Peptide. *Small* **2009**, *5* (13), 1562–1568. https://doi.org/10.1002/smll.200900186.

(8)   Hoshino, Y.; Koide, H.; Furuya, K.; Haberaecker, W. W.; Lee, S.-H.; Kodama, T.; Kanazawa, H.; Oku, N.; Shea, K. J. The Rational Design of a Synthetic Polymer Nanoparticle That Neutralizes a Toxic Peptide in Vivo. *Proc. Natl. Acad. Sci.* **2012**, *109* (1), 33–38. https://doi.org/10.1073/pnas.1112828109.

(9)   Hoshino, Y.; Taniguchi, S.; Takimoto, H.; Akashi, S.; Katakami, S.; Yonamine, Y.; Miura, Y. Homogeneous Oligomeric Ligands Prepared via Radical Polymerization That Recognize and Neutralize a Target Peptide. *Angew. Chem.* **2020**, *132* (2), 689–693. https://doi.org/10.1002/ange.201910558.

(10) O'Brien, J.; Lee, S.-H.; Gutiérrez, J. M.; Shea, K. J. Engineered Nanoparticles Bind Elapid Snake Venom Toxins and Inhibit Venom-Induced Dermonecrosis. *PLoS Negl. Trop. Dis.* **2018**, *12* (10), e0006736. https://doi.org/10.1371/journal.pntd.0006736.

(11) Koide, H.; Hirano, S.; Ide, T.; Saito, K.; Suzuki, H.; Yasuno, G.; Hamashima, Y.; Yonezawa, S.; Oku, N.; Asai, T. Engineering of Lipid Nanoparticles by the Multifunctionalization of the Surface with Amino Acid Derivatives for the Neutralization of a Target Toxic Peptide. *Adv. Funct. Mater.* **2021**, *31* (3), 2005641. https://doi.org/10.1002/adfm.202005641.

(12) Koide, H.; Suzuki, H.; Ochiai, H.; Egami, H.; Hamashima, Y.; Oku, N.; Asai, T. Enhancement of Target Toxin Neutralization Effect in Vivo by PEGylation of Multifunctionalized Lipid Nanoparticles. *Biochem. Biophys. Res. Commun.* **2021**, *555*, 32–39. https://doi.org/10.1016/j.bbrc.2021.03.073.

(13) Koide, H.; Yamauchi, I.; Hoshino, Y.; Yasuno, G.; Okamoto, T.; Akashi, S.; Saito, K.; Oku, N.; Asai, T. Design of Abiotic Polymer Ligand-Decorated Lipid Nanoparticles for Effective Neutralization of Target Toxins in the Blood. *Biomater. Sci.* **2021**, *9* (16), 5588–5598. https://doi.org/10.1039/D1BM00515D.

(14) Xiao, R. Z.; Zeng, Z. W.; Zhou, G. L.; Wang, J. J.; Li, F. Z.; Wang, A. M. Recent Advances in PEG–PLA Block Copolymer Nanoparticles. *Int. J. Nanomedicine* **2010**, *5*, 1057–1065. https://doi.org/10.2147/IJN.S14912.

(15) Wang, C.-W.; Sinton, D.; Moffitt, M. G. Flow-Directed Block Copolymer Micelle Morphologies via Microfluidic Self-Assembly. *J. Am. Chem. Soc.* **2011**, *133* (46), 18853–18864. https://doi.org/10.1021/ja2067252.

(16) Feng, H.; Lu, X.; Wang, W.; Kang, N.-G.; Mays, J. W. Block Copolymers: Synthesis, Self-Assembly, and Applications. *Polymers* **2017**, *9* (10), 494. https://doi.org/10.3390/polym9100494.

(17) Blanazs, A.; Armes, S. P.; Ryan, A. J. Self-Assembled Block Copolymer Aggregates: From Micelles to Vesicles and Their Biological Applications. *Macromol. Rapid Commun.* **2009**, *30* (4–5), 267–277. https://doi.org/10.1002/marc.200800713.

(18) Otsuka, H.; Nagasaki, Y.; Kataoka, K. Self-Assembly of Poly(Ethylene Glycol/ -Based Block Copolymers for Biomedical Applications. *Interface Sci.* **2001**, 8.

(19) Emoto, K.; Nagasaki, Y.; Kataoka, K. Coating of Surfaces with Stabilized Reactive Micelles from Poly(Ethylene Glycol)−Poly(DL -Lactic Acid) Block Copolymer. *Langmuir* **1999**, *15* (16), 5212–5218. https://doi.org/10.1021/la980918s.

(20) Yamamoto, Y.; Yasugi, K.; Harada, A.; Nagasaki, Y.; Kataoka, K. Temperature-Related Change in the Properties Relevant to Drug Delivery of Poly(Ethylene Glycol)–Poly(d,l-Lactide) Block Copolymer Micelles in Aqueous Milieu. *J. Controlled Release* **2002**, *82* (2–3), 359–371. https://doi.org/10.1016/S0168-3659(02)00147-5.

(21) Chen, H.; Kim, S.; He, W.; Wang, H.; Low, P. S.; Park, K.; Cheng, J.-X. Fast Release of Lipophilic Agents from Circulating PEG-PDLLA Micelles Revealed by *in Vivo* Förster Resonance Energy Transfer Imaging. *Langmuir* **2008**, *24* (10), 5213–5217. https://doi.org/10.1021/la703570m.

(22) Zhou, H.; Fan, Z.; Li, P. Y.; Deng, J.; Arhontoulis, D. C.; Li, C. Y.; Bowne, W. B.; Cheng, H. Dense and Dynamic Polyethylene Glycol Shells Cloak Nanoparticles from Uptake by Liver Endothelial Cells for Long Blood Circulation. *ACS Nano* **2018**, *12* (10), 10130–10141. https://doi.org/10.1021/acsnano.8b04947.

(23) Garofalo, C.; Capuano, G.; Sottile, R.; Tallerico, R.; Adami, R.; Reverchon, E.; Carbone, E.; Izzo, L.; Pappalardo, D. Different Insight into Amphiphilic PEG-PLA Copolymers: Influence of Macromolecular Architecture on the Micelle Formation and Cellular Uptake. *Biomacromolecules* **2014**, *15* (1), 403–415. https://doi.org/10.1021/bm401812r.

(24) Joseph R. Lakowicz. Introduction to Fluorescence. In *Principles of Fluorescence Spectroscopy*; Springer New York, NY; pp 1–26.

(25) Chen, T.; He, B.; Tao, J.; He, Y.; Deng, H.; Wang, X.; Zheng, Y. Application of Förster Resonance Energy Transfer (FRET) Technique to Elucidate Intracellular and In Vivo Biofate of Nanomedicines. *Adv. Drug Deliv. Rev.* **2019**, *143*, 177–205. https://doi.org/10.1016/j.addr.2019.04.009.

(26) Sahoo, H. Förster Resonance Energy Transfer – A Spectroscopic Nanoruler: Principle and Applications. *J. Photochem. Photobiol. C Photochem. Rev.* **2011**, *12* (1), 20–30. https://doi.org/10.1016/j.jphotochemrev.2011.05.001.

(27) Mooney, A. M. *FRET Jablonski Diagram with Typical Timescales.*; 2012.

(28) Zou, P.; Chen, H.; Paholak, H. J.; Sun, D. Noninvasive Fluorescence Resonance Energy Transfer Imaging of *in Vivo* Premature Drug Release from Polymeric Nanoparticles. *Mol. Pharm.* **2013**, *10* (11), 4185–4194. https://doi.org/10.1021/mp4002393.

(29) Xie, M.; Wang, S.; Singh, A.; Cooksey, T. J.; Marquez, M. D.; Bhattarai, A.; Kourentzi, K.; Robertson, M. L. Fluorophore Exchange Kinetics in Block Copolymer Micelles with Varying Solvent–Fluorophore and Solvent–Polymer Interactions. *Soft Matter* **2016**, *12* (29), 6196–6205. https://doi.org/10.1039/C6SM00297H.

(30) Jiwpanich, S.; Ryu, J.-H.; Bickerton, S.; Thayumanavan, S. Noncovalent Encapsulation Stabilities in Supramolecular Nanoassemblies. *J. Am. Chem. Soc.* **2010**, *132* (31), 10683–10685. https://doi.org/10.1021/ja105059g.

(31) Jenkins, T.; Fryer, T.; Dehli, R.; Jürgensen, J.; Fuglsang-Madsen, A.; Føns, S.; Laustsen, A. Toxin Neutralization Using Alternative Binding Proteins. *Toxins* **2019**, *11* (1), 53. https://doi.org/10.3390/toxins11010053.

(32) Weisman, A.; Chou, B.; O'Brien, J.; Shea, K. J. Polymer Antidotes for Toxin Sequestration. *Adv. Drug Deliv. Rev.* **2015**, *90*, 81–100. https://doi.org/10.1016/j.addr.2015.05.011.

(33) Raghuraman, H.; Chattopadhyay, A. Melittin: A Membrane-Active Peptide with Diverse Functions. *Biosci. Rep.* **2007**, *27* (4–5), 189–223. https://doi.org/10.1007/s10540-006-9030-z.

(34) Lee, M.-T.; Sun, T.-L.; Hung, W.-C.; Huang, H. W. Process of Inducing Pores in Membranes by Melittin. *Proc. Natl. Acad. Sci.* **2013**, *110* (35), 14243–14248. https://doi.org/10.1073/pnas.1307010110.

(35) Peraro, M. D.; van der Goot, F. G. Pore-Forming Toxins: Ancient, but Never Really out of Fashion. *Nat. Rev. Microbiol.* **2016**, *14* (2), 77–92. https://doi.org/10.1038/nrmicro.2015.3.

(36) Kang, T.; Li, C.; Du, T.; Wu, Y.; Yang, Y.; Liu, X.; Zhang, Q.; Xu, X.; Gou, M. A Biomimetic Nanoparticle-Enabled Toxoid Vaccine against Melittin. *Int. J. Nanomedicine* **2018**, *13*, 3251–3261. https://doi.org/10.2147/IJN.S156346.

(37) Tao, J.; Xu, X.; Liu, H.; Jiang, X.; Mao, J.; Gou, M. A Nanoparticle-Functionalized Wound Dressing Device for Toxin Neutralization. *Mater. Des.* **2020**, *188*, 108431. https://doi.org/10.1016/j.matdes.2019.108431.

(38) Los, F. C. O.; Randis, T. M.; Aroian, R. V.; Ratner, A. J. Role of Pore-Forming Toxins in Bacterial Infectious Diseases. *Microbiol. Mol. Biol. Rev. MMBR* **2013**, *77* (2), 173–207. https://doi.org/10.1128/MMBR.00052-12.

(39) van den Bogaart, G.; Guzmán, J. V.; Mika, J. T.; Poolman, B. On the Mechanism of Pore Formation by Melittin. *J. Biol. Chem.* **2008**, *283* (49), 33854–33857. https://doi.org/10.1074/jbc.M805171200.

(40) Laustsen, A. H.; María Gutiérrez, J.; Knudsen, C.; Johansen, K. H.; Bermúdez-Méndez, E.; Cerni, F. A.; Jürgensen, J. A.; Ledsgaard, L.; Martos-Esteban, A.; Øhlenschlæger, M.; Pus, U.; Andersen, M. R.; Lomonte, B.; Engmark, M.; Pucca, M. B. Pros and Cons of Different Therapeutic Antibody Formats for Recombinant Antivenom Development. *Toxicon* **2018**, *146*, 151–175. https://doi.org/10.1016/j.toxicon.2018.03.004.

(41) Chen, H.; Kim, S.; Li, L.; Wang, S.; Park, K.; Cheng, J.-X. Release of Hydrophobic Molecules from Polymer Micelles into Cell Membranes Revealed by Förster Resonance Energy Transfer Imaging. *Proc. Natl. Acad. Sci.* **2008**, *105* (18), 6596–6601. https://doi.org/10.1073/pnas.0707046105.